Modeling solar zenith angle effects on the polar wind

A. Glocer,[1] N. Kitamura,[2] G. Toth,[3] and T. Gombosi[3]

Received 6 September 2011; revised 13 March 2012; accepted 15 March 2012; published 25 April 2012.

[1] We use the Polar Wind Outflow Model (PWOM) to study the geomagnetically quiet conditions in the polar cap during solar maximum. The PWOM solves the gyrotropic transport equations for O^+, H^+, and He^+ along several magnetic field lines in the polar region in order to reconstruct the full 3D solution. We directly compare our simulation results to the data based empirical model of Kitamura et al. (2011) of electron density which is based on 63 months of Akebono satellite observations. The modeled ion and electron temperatures are also compared with a statistical compilation of quiet time data obtained by the EISCAT Svalbard Radar (ESR) and Intercosmos Satellites. The data and model agree reasonably well, albeit with some differences. This study shows that photoelectrons play an important role in explaining the differences between sunlit and dark results of electron density, ion composition, as well as ion and electron temperatures of the quiet time polar wind solution. Moreover, these results provide an initial validation of the PWOM's ability to model the quiet time "background" solution.

Citation: Glocer, A., N. Kitamura, G. Toth, and T. Gombosi (2012), Modeling solar zenith angle effects on the polar wind, *J. Geophys. Res.*, *117*, A04318, doi:10.1029/2011JA017136.

1. Introduction

[2] The existence of ionospheric outflows of plasma to the magnetosphere along open magnetic field lines, known as the polar wind, was first suggested by *Axford* [1968] and *Banks and Holzer* [1968]. This suggestion was later confirmed by observations by the Explorer 31 and ISIS 2 satellites [*Hoffman*, 1970; *Brinton et al.*, 1971; *Hoffman et al.*, 1974]. The Retarding Ion Mass Spectrometer (RIMS) on board the Dynamics Explorer 1 (DE-1) satellite provided the first quantitative observations of H^+ and O^+ flows [*Nagai et al.*, 1984; *Waite et al.*, 1985]. While the polar wind was originally thought of as an consisting of light ions, calculations by *Barakat and Schunk* [1983] demonstrated that O^+ could comprise a significant portion of the polar wind when the electron temperature is high. Indeed, observations by the Akebono satellite has demonstrated the presence of a large number of O^+ ions in the polar wind [*Abe et al.*, 1993]. The established presence of O^+ in the polar wind is indicative of the importance of nonclassical processes.

[3] Photoelectrons formed from ionization of the atmosphere by solar radiation can have a significant effect on the polar wind solution. *Axford* [1968] and *Lemaire* [1972] suggested that escaping photoelectrons can drag ions away from the upper atmosphere. The study by *Lemaire* [1972], however, only considered fairly low concentrations of photoelectrons, and therefore gave results of a classical polar wind dominated by H^+ at high altitudes. Numerical simulations of the effect of photoelectrons on the polar wind by *Tam et al.* [1995, 1998] showed that the presence of photoelectrons can strongly influence the O^+ solution, but their solution also predicted a localized electron temperature of more than 40,000 Kelvin. Simulations by *Khazanov et al.* [1997] have also shown that photoelectrons play an important role in the polar wind O^+ and H^+ solution, but without the localized electron temperature enhancement and with weaker ion acceleration. Other simulation studies by *Wilson et al.* [1997] and *Su et al.* [1998] have found similar results and further investigated the consequences of a potential drop above three Earth radii.

[4] Satellite observations show that the photoelectron flux exhibits a clear Solar Zenith Angle (SZA) dependence [*Lee et al.*, 1980; *Peterson et al.*, 2008], which may result in SZA effect in the polar wind solution. Although the SZA dependence of many polar wind quantities have not been determined, there have been some studies of the SZA dependence of the electron density in the polar region.

[5] More recently *Kitamura et al.* [2011] presented an empirical model of the electron density profile during geomagnetically quiet time as a function of solar zenith angle. This model is derived from 63 months of Akebono satellite observations at solar maximum, and spans an altitude range of 500 km to 10,500 km. They demonstrate a clear sunlit-dark transition in the altitude profile of the electron density. They also use EISCAT Svalbard Radar (ESR) and Intercosmos (IK) satellite data to demonstrate a strong change in the electron and ion temperatures near the terminator. Additionally, by comparing their results with modeling studies they made a most intriguing inference: under sunlit conditions O^+ is the dominant ion up to at least 10,500 km during geomagnetically quiet times. The present study uses modeling to throughly explore these results.

[1]NASA GSFC, Greenbelt, Maryland, USA.
[2]Department of Geophysics, Tohoku University, Sendai, Japan.
[3]Department of Atmospheric Oceanic and Space Science, University of Michigan, Ann Arbor, Michigan, USA.

0148-0227/12/2011JA017136

[6] A detailed description of our modeling set up is provided in section 2, and the event details and results are given in section 3. We summarize our results and discuss our conclusions in section 4.

2. Model Details

[7] The Polar Wind Outflow Model (PWOM) [*Glocer et al.*, 2007, 2009a, 2009b] is the main modeling tool of this study. It determines the solution of ionospheric H^+, O^+, He^+ and electrons in the transition region between the magnetosphere and ionosphere. The lower bound of the PWOM is located firmly in the ionosphere at 250 km above the Earth's surface, while the upper boundary is in the magnetosphere at a few Earth radii. The complete three dimensional solution is obtained by solving the full field-aligned gyrotropic transport equations for multiple ions along field lines convecting through the polar cap. However, in this study we hold the lines stationary. Figure 1 is meant to illustrates how solutions along multiple field lines can be combined to reconstruct the 3D solution.

[8] The ionospheric boundary conditions are set to have zero field-aligned velocity, ion and electron temperatures equal to the neutral temperature, and a chemical equilibrium solution for the ion densities. In this study, we use the MSIS-90 (mass spectrometer and incoherent scatter) empirical model [*Hedin*, 1983, 1987, 1991] to obtain the neutral densities and temperatures.

[9] The idea that energetic photoelectrons can cause strong ambipolar electric fields resulting in heavy ion outflows was proposed by *Axford* [1968]. Subsequent modeling studies have shown that photoelectrons can indeed have an effect [*Tam et al.*, 1995; *Khazanov et al.*, 1997]. Our recent efforts build on this past work by including photoelectrons into our 3D picture.

[10] Photoelectrons are included into the PWOM calculation using three steps:

[11] 1. We define the photoelectron distribution at the base of each field line based on the 2 stream calculation of *Su et al.* [1998], which is based on work by *Banks and Nagy* [1970].

[12] 2. The photoelectron flux as a function of altitude is found using an analytical solution based on the technique described by *Khazanov et al.* [1997].

[13] 3. The photoelectron flux is then incorporated into the PWOM calculation by modifying the electron continuity (equation (2)) and momentum (equation (3)) equations to include photoelectrons as well as thermal electrons.

[14] Figure 2 presents the photoelectron flux and characteristic energy calculated by *Su et al.* [1998] and used to define the photoelectron distribution at the base of each of our field lines. The values are given as a function of solar zenith angle for two values of F10.7: 90 and 200 (10^{-22} Wm^{-2} Hz^{-1}). The lower value reflects the solution for solar minimum and the higher value reflects the solution for solar maximum. In this paper, we only make use of the solar maximum case.

[15] The photoelectron flux along a field line is found using an analytical solution of the steady state collisionless kinetic equation

$$\mu v\frac{\partial f_\alpha}{\partial r}-\frac{1-\mu^2}{2B}\frac{\partial B}{\partial r}v\frac{\partial f_\alpha}{\partial \mu}=-\left(\frac{e}{m_e}E_\parallel-g\right)\left(\mu\frac{\partial f_\alpha}{\partial v}+\frac{1-\mu^2}{v}\frac{\partial f_\alpha}{\partial \mu}\right) \quad (1)$$

presented by *Khazanov et al.* [1997]. Where μ is the cosine of the pitch angle, v is velocity, f_α is the photoelectron distribution function, r is the radial distance, e is the electron charge, m_e is the electron mass, $E_\parallel$ is the ambipolar electric field, B is the magnetic field, and g is the gravitational acceleration. Three important assumptions are involved in finding the solution to this equation. The photoelectron source population is represented as a upper half Maxwellian, the effects of collisions are neglected, and the solution is broken into transient and reflected populations. The full solution is too long to reproduce here, but is explicitly spelled out by *Khazanov et al.* [1997].

[16] To include the effect of photoelectrons into the PWOM calculation we split the electron population in to two pieces: thermal and photoelectrons. Unlike the ions, the electrons are not solved using the full transport equations. Rather, they are solved using charge neutrality, a steady state electron velocity assumption, and an energy equation [*Gombosi and Nagy*, 1989]

$$n_e+n_\alpha=\sum_i n_i \quad (2)$$

$$n_e u_e+n_\alpha u_\alpha=\left(\sum_i n_i u_i-\frac{j}{e}\right) \quad (3)$$

$$j=j_0\frac{A_0}{A} \quad (4)$$

$$\rho_e\frac{\partial T_e}{\partial t}=(\gamma_e-1)\frac{m_e}{kA}\frac{\partial}{\partial r}\left(A\kappa_e\frac{\partial T_e}{\partial r}\right)-\rho_e u_e\frac{\partial T_e}{\partial r}-T_e\left[S_e+\frac{\gamma_e-1}{A}\rho_e\frac{\partial}{\partial r}(Au_e)\right]+(\gamma_e-1)\frac{m_e}{k}\frac{\delta E_e}{\delta t}, \quad (5)$$

where n_e, n_α, and n_i are the densities of the thermal electrons, photoelectrons, and ions species, respectively. ρ_e is the thermal electron mass density, A is the cross section area of the flux tube, u_i is the bulk velocity of an ion species, u_e is the bulk velocity of the thermal electrons, u_α is the bulk velocity of the photoelectrons, $\delta E_e/\delta t$ is a source term, j is the current density, k is Boltzmann's constant, and the subscript 0 represents the value taken at a reference altitude.

[17] The ambipolar electric field is calculated in the following manner [*Gombosi and Nagy*, 1989]:

$$E_\parallel=-\frac{1}{en_e}\left[\frac{\partial}{\partial r}\left(p_e+\rho_e u_e^2\right)+\frac{A'}{A}\rho_e u_e^2\right]+\frac{1}{en_e}\frac{\partial}{\partial r}\left(\sum_i\frac{m_e}{m_i}\left[(u_e-u_i)S_i-\frac{\delta M_i}{\delta t}\right]+\frac{\delta M_e}{\delta t}\right) \quad (6)$$

T_i is the ion temperature, m_i is the ion mass, S_i is the mass source rate, and $\frac{\delta M}{\delta t}$ is the momentum exchange rate.

[18] Equations (5) and (6) [from *Gombosi and Nagy*, 1989] are found from a simplification of the full electron energy and momentum equation in the gyrotropic assumption. The assumptions in this simplification are that the electron density and velocity can be approximately described by a steady state (from quasi-neutrality and ion flux/current balance) but the temperature is time dependent. The mass, momentum and energy source terms in these equations are determined by using Burgers' fully linear approximation

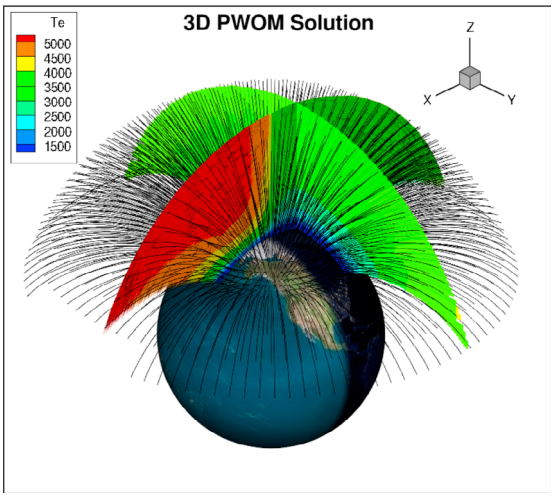

Figure 1. A 3-D representation of the Polar Wind Outflow Model (PWOM) calculation. The more than 900 black lines represent individual field lines in the computation, while the colored contour slices show the 3-D reconstruction of electron temperature.

[*Burgers*, 1969]. The specific expression for the momentum exchange rate is given by *Schunk and Nagy* [2000] as

$$\frac{\delta M_i}{\delta t} = -\sum_j \rho_i \nu_{ij} (u_i - u_j) \tag{7}$$

and $\frac{\delta E}{\delta t}$ is the energy exchange rate is given by *Schunk and Nagy* [2000] as

$$\frac{\delta E_i}{\delta t} = \sum_j \frac{\rho_i \nu_{ij}}{m_i + m_j} \left[3k(T_j - T_i) + m_j (u_i - u_j)^2 \right], \tag{8}$$

where i and j refers to species (ions or electron) and ν_{ij} is the collision frequency. The mass source rate is determined by the production and loss rates from photoionization and chemical kinetics.

[19] For the simulations in this study, we use a 'stripped down' version of the model in order to reduce the complexity of the solution and focus on the role of specific processes. Specifically, we hold our field lines stationary and do not allow them to convect with convection velocity defined from the polar cap potential. The input F10.7 and Ap index are also fixed in time to represent solar maximum geomagnetically quiet conditions. Furthermore, the topside electron heat flux input, which is usually modulated based on electron precipitation inputs is held to the same low fixed value for all field lines. Finally, the formulation of our equations implicitly assumes that field lines are straight and vertical which is an approximation that loses validity the further they are from the poles. While the field lines in our study are at high and midlatitude, we hope to improve on this formulation in future studies.

[20] In summary, our modeling approach solves the polar wind solution along multiple field lines to obtain the three dimensional solution. We use a time-dependent transport equation for the ions including mass sources, collisions, and heat flow [*Gombosi and Nagy*, 1989]. A steady state collisionless kinetic solution for the photoelectrons, using the analytical solution of *Khazanov et al.* [1997], gives the photoelectron solution along the field line. The quasi-neutrality and current conservation equations include both thermal and photoelectrons (as in the approach of *Khazanov et al.* [1997]). A time-dependent electron temperature equation is used. Although the approach for including photoelectrons is adapted from the approach of *Khazanov et al.* [1997] there are three main differences between our model and theirs for obtaining the solution along a particular field line which can be summarized as follows: (1) They use a kinetic approach for the ions while we use transport equations, (2) they use steady state solution for the ions and thermal electron temperature while we use time-dependent

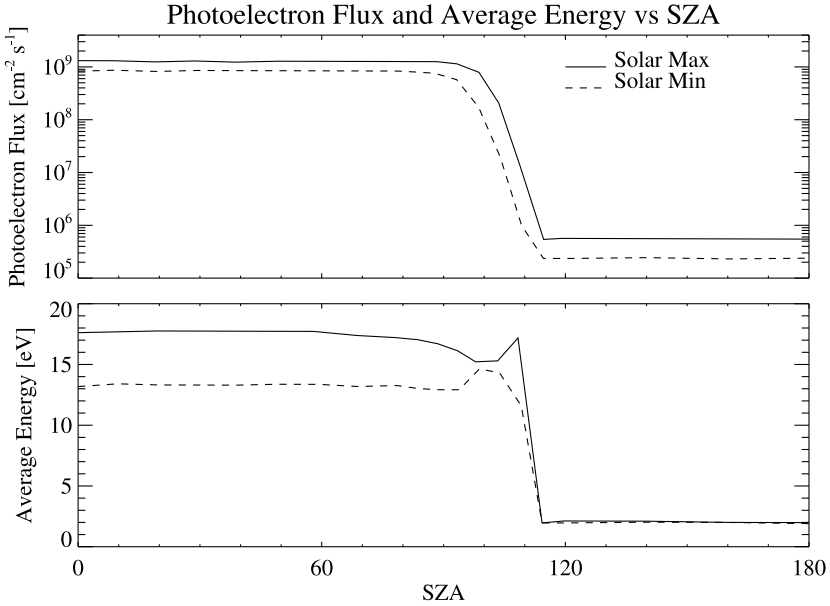

Figure 2. The photoelectron inputs used by PWOM as a function of Solar Zenith Angle (SZA) (adapted from *Su et al.* [1998]). Photoelectron flux and energy are given for solar maximum and solar minimum.

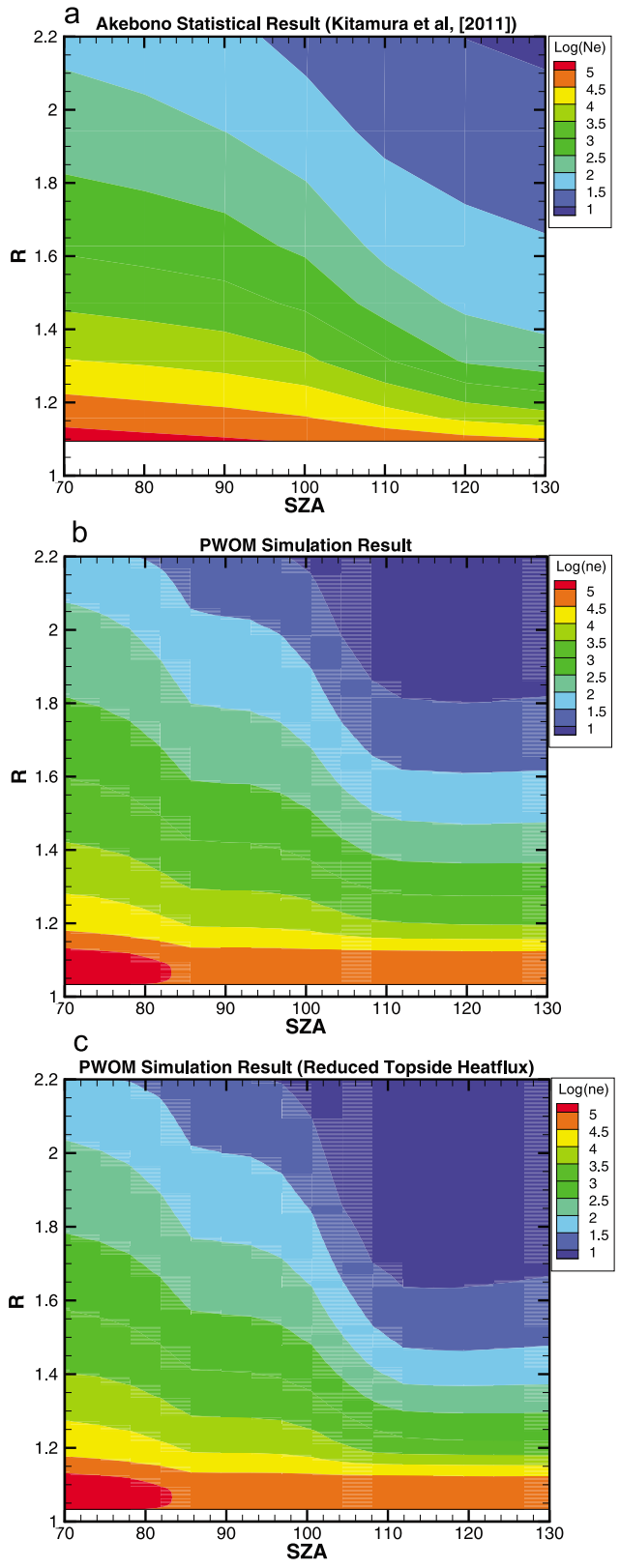

Figure 3. The log of the electron density (in cm^{-3}) as a function of solar zenith angle and distance from the center of the planet. (a) The result based on Akebono data [*Kitamura et al.*, 2011], (b) the result of the PWOM calculation, and (c) the result of the PWOM calculation with reduced topside electron heat flux.

equations, and (3) their equations do not include collisions or other sources while ours does. We call these points out in order clarify the differences between the models.

3. Results

[21] We apply our model to explain observations in the high-altitude polar cap. In particular, we compare our calculation to an empirical model of electron density based on Akebono observations as well as ion and electron temperature data from the EISCAT Svalbard Radar (ESR) and the Intercosmos-24 (IK-24) and Intercosmos-25 (IK-25) satellites.

[22] *Kitamura et al.* [2011] present an empirical model of the electron density profile during geomagnetically quiet time as a function of solar zenith angle. This model is derived from 63 months of Akebono satellite observations at solar maximum, and spans an altitude range of 500 km to 10,500 km. The superposition of a hydrostatic term ($N1 = n_{500}\exp(1.08(500 - z)/(rh_{500}))$) and a power law term ($N2 = n_{10000}(r/2.57)^{-\alpha}$) gives the empirical model (N1 + N2). The values n_{500}, h_{500}, n_{10000}, and α are chosen to give the best fit to the data. Only the data in the polar cap is included; the cusp and auroral zone are not. This gives a picture of the background quiet time solution in the high-altitude, high-latitude ionosphere. Figure 3a shows the result of this empirical model in the form of a color contour plot of the log of the electron density as a function of Solar Zenith Angle (SZA) and radial distance from the center of the Earth (r). The SZA in Figure 3a is that at the magnetic foot point.

[23] Figure 3b presents the result of a PWOM simulation showing the log of the electron number density as a function of SZA and R. The simulation is for solar maximum conditions (F10.7 = 200) and geomagnetically quiet conditions (Ap = 5) with no convection in the polar cap. The simulation is done for a typical fall day, although similar results are found for other seasons. 906 field lines distributed around the polar cap were used in the simulation. To generate Figure 3b, we bin all the solution points along all the field lines in SZA (at base of the field line) and r; the values in each of those bins are then averaged.

[24] Since Figures 3a and 3b are in the exact same format, they can be directly compared. We find that qualitatively the two results are in reasonable agreement. In both plots, the electron density drops off more slowly with altitude on the dayside and faster on the nightside. This transition is most strongly visible as the SZA increases from 90 to 110 degrees. The two results are seen to differ most significantly in the high altitude, high SZA region where the densities are the lowest.

[25] Figure 3c presents the result of a PWOM simulation with the topside electron heat flux reduced by a factor of two. The purpose of including this case is to examine the role of topside electron heat flux in the calculation. We see that the solution in Figure 3c is very similar to the solution in Figure 3b; both solutions show a transition across the terminator and have nearly identical solutions under sunlit conditions. The main difference is seen in the vertical profile of the electron density at large solar zenith angles. This indicates that the solution is more sensitive to the topside electron heat flux under dark conditions than sunlit conditions. We note that the topside electron heat flux is an ill

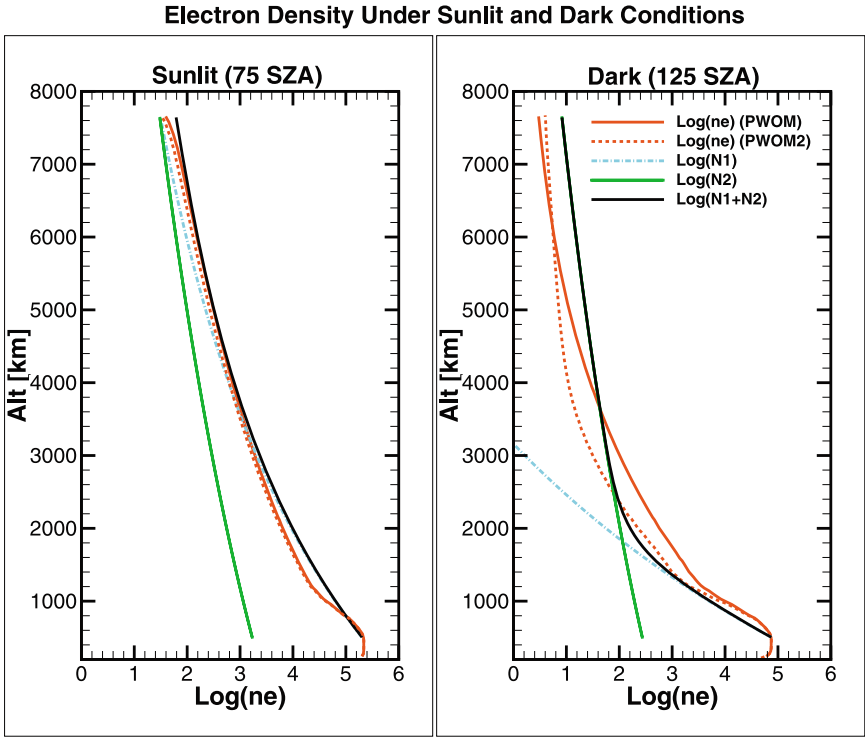

Figure 4. A direct comparison between the PWOM calculation of N_e (orange) and the empirical fit (black) of *Kitamura et al.* [2011] at 75° SZA and 125° SZA. N1 = $n_{500}\exp(1.08(500 - z)/(rh_{500}))$ (cyan) is the hydrostatic term and N2 = $n_{10000}(r/2.57)^{-\alpha}$ (green) is the power law term in the empirical fit. The result of a PWOM simulation with the topside electron heat flux reduced by a factor of two (orange dashed) is also shown. (left) Sunlit and (right) dark conditions are shown.

constrained quantity (in that there are no measurements of this parameter) and the default value was chosen to give reasonable agreement, however it may not have been the ideal choice.

[26] Figure 4 takes a closer look at the vertical profile of electron density under sunlit and dark conditions. Figure 4 (left) shows the result for sunlit conditions (75° SZA), and Figure 4 (right) shows the solution for dark conditions (125° SZA). The PWOM solution is shown in orange and the data based empirical model is shown in black. The PWOM solution with reduced topside electron heat flux is shown with an orange dashed line. Our simulation result is found by extracting the solution at a particular SZA from Figures 3b and 3c. Also shown are the hydrostatic (cyan) and the power law (green) terms in the empirical model. The hydrostatic term is seen to dominate under sunlit conditions at all altitudes, while under dark conditions the power law term becomes dominant above 2000 km. The PWOM result agrees well with the empirical fit at all altitudes under sunlit conditions. The agreement is still reasonably good under dark conditions, but differences are clearly seen at high altitudes. This discrepancy may be due to the limitations inherent to the fluid-like approach used in our model, or the high-altitude processes that are missing from it. These differences are fairly small in absolute terms but are significant in relative terms.

[27] We also use our model to examine a statistical compilation of ion and electron temperatures presented by *Kitamura et al.* [2011]. The data are derived from two sources: EISCAT Svalbard Radar (ESR) and Intercosmos 24 and 25 (IK-24 and IK-25) satellites. The ESR takes measurements at the 75° invariant latitude. The ESR data used is composed of 639 observations over 19 months between February 2000 and May 2002. The IK-24 and IK-25 satellites obtain the electron temperature from radio frequency probes. The IK data used is comprised of 26 months of IK-24 and 4 months of IK-25 observations that satisfy the criterion for solar maximum. For further details of these data sets, refer to the work of *Kitamura et al.* [2011].

[28] Figure 5 compares the PWOM calculation of electron (pink) and ion (green) temperatures with ESR electron (red) and ion (cyan) temperatures. The PWOM simulation with reduced topside electron heat flux is shown with dashed lines. Also compared are the electron temperatures from the Intercosmos (IK) satellites (black). We note that the ESR and IK data represent solutions in a SZA range, and the PWOM solution we are comparing with is the solution in the middle of that range. The ion temperatures calculated by PWOM exhibit good agreement with the data under both sunlit and dark conditions. The electron temperature calculated by PWOM exhibits similar behavior to the data, albeit with some differences. Under sunlit conditions, the modeled electron temperature is seen to be somewhat too low below about 500 km and also reaches moderately higher values than is observed at high altitudes. Additionally, while the data show the electron temperature to be fairly constant above 500 km, the electron temperature in the model continues to increase with altitude. Both the model and the data

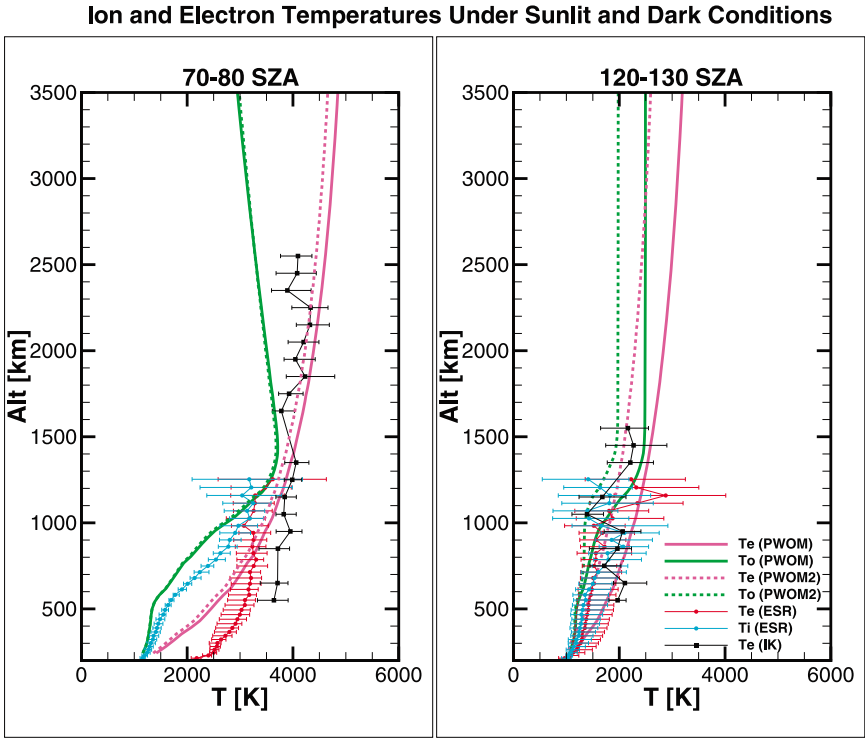

Figure 5. A direct comparison between the PWOM calculation of electron (purple) and ion (green) temperatures with EISCAT Svalbard Radar (ESR) electron (red) and ion (blue) temperatures. Also compared are the electron temperatures from the Intercosmos (IK) satellites (black); only the bins with the pass number larger than 5 are plotted. The ESR and IK data are taken from *Kitamura et al.* [2011]. (left) Sunlit and (right) dark conditions are shown.

demonstrate that the electron and ion temperatures are higher under sunlit conditions as compared to dark conditions.

[29] We examine the transition from sunlit to dark conditions by comparing the model and data at a fixed altitude for different solar zenith angles. Figure 6 presents these results in a plot of temperature vs SZA. The PWOM results are taken at 800 km, the ESR data are from 700–800 km, and the IK data are from 500–1000 km. In both the model and the data, a sharp transition is seen at a SZA of 100°. The transition is most pronounced in the electron temperature, while the ion temperature exhibits a more gradual decline across the terminator. The PWOM results are found qualitatively consistent with the ESR and IK data.

[30] In their study, *Kitamura et al.* [2011] posit that the day-night asymmetry of the electron density is due to different ion composition under sunlit and dark conditions. They claim that O^+ ions are dominant up to at least 10,500 km altitude on the dayside, but H^+ ions are dominant at high altitudes on the nightside. This assertion comes from two sources. First, the hydrostatic term in their fit dominates to approximately 8000 km altitude in sunlit conditions, while the power law term dominates at high altitudes in dark conditions. Secondly, comparisons with a model containing photoelectrons [*Wilson et al.*, 1997], which has O^+ as the dominant species to high altitude, show reasonable agreement with the sunlit empirical results; comparisons with models that do not include photoelectrons [*Schunk*, 1981; *Schunk and Watkins*, 1982; *Mitchell and Palmadesso*, 1983; *Ganguli et al.*, 1987] show reasonable agreement with the empirical results for dark conditions, and those models primarily consist of H^+ at high altitudes. As a result, they conclude that the O^+ density in the polar wind is controlled by solar inputs.

[31] Our model can directly test this hypothesis by looking at the percent of O^+ as a function of SZA and R. Figure 7 presents exactly this information. Figure 7 clearly shows that the sunlit portion of the modeled solution is primarily populated by O^+. The dark portion of the modeled domain is mostly H^+ above 5500 km and O^+ below. A clear transition is visible across the terminator beginning at a SZA of approximately 95° and ending at about a SZA of 110°.

[32] We strengthen this conclusion by comparing our model's results to past studies. Figure 8 shows this comparison. Figure 8 (left) shows the altitude profile of the log of electron density for our PWOM results (blue), the results from *Wilson et al.* [1997] (red), the results from *Khazanov et al.* [1997] with 0.1% concentration of photoelectrons (pink), and the results from *Lemaire* [1972] (green). The empirical model (black) is included as a reference. Solid lines represent results appropriate for sunlit conditions, and dashed lines are results for dark conditions. Figure 8 (right) shows the percentage of O^+ in the solutions as a function of altitude. We find that our modeling results of the log of the electron density agree favorably with both the empirical fit to the Akebono data and with past models. Moreover, our conclusion that O^+ is the dominant constituent under

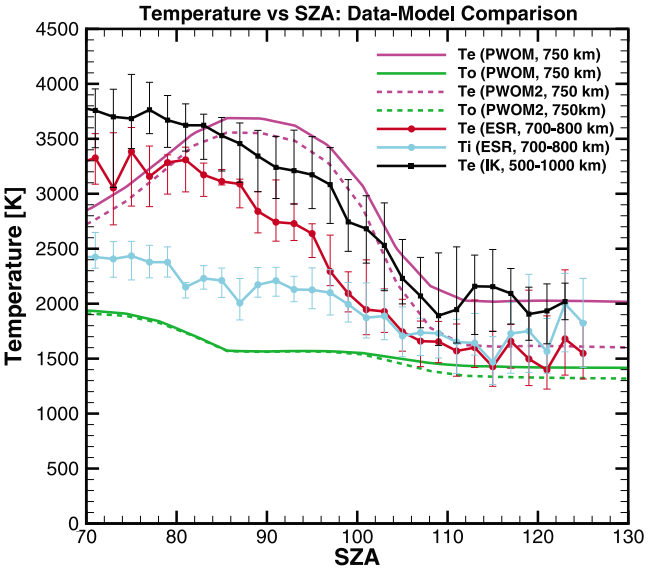

Figure 6. A direct comparison as a function of SZA at fixed altitude between the PWOM calculation of electron (purple) and ion (green) temperatures with ESR electron (red) and ion (blue) temperatures. Also compared are the electron temperatures from the Intercosmos (IK) satellite (black); only the bins with the pass number larger than 5 are plotted. The dashed lines show the result of a PWOM simulation with the topside heat electron heat flux reduced by a factor of 2. The ESR and IK data are taken from *Kitamura et al.* [2011].

geomagnetically quiet sunlit conditions is consistent with the results of *Wilson et al.* [1997] and *Khazanov et al.* [1997]. The conclusion that H^+ dominates at high altitude during geomagnetically quiet dark conditions is in agreement with the result of *Lemaire* [1972]. Although the study by *Lemaire* [1972] includes photoelectrons, the concentrations are very low (≤0.0094% at 1000 km). Therefore we consider this solution most appropriate for large SZA values seen under dark conditions.

[33] The change in the vertical profile of the electron density and the O^+ composition between sunlit and dark conditions is largely driven by two different but closely tied mechanisms, namely, photoelectrons and the enhancement of the O^+ production rate. From the observational point of view, it is almost impossible to distinguish between the effects of these two mechanisms. However, using our model we can examine the contribution of each mechanism separately, and hence evaluate their relative importance. Figure 9 shows the result of these tests where the red colored lines show the result with a changing O^+ production rate but no photoelectrons, the green colored lines show the result with photoelectrons but with the production rate fixed to a 'dark' value, and the blue colored lines show the result with both effects included. The result of *Kitamura et al.* [2011] is shown in black. Results for sunlit conditions are solid while the dashed lines represent the dark solution. As expected, the solution under dark conditions is the same for all cases, but the solution under sunlit conditions is altered. In particular, the density at high altitudes is decreased by approximately an order of magnitude when photoelectrons are not included. The density is also decreased at high altitudes when the O^+ production rate is held to dark values (but photoelectrons are included), however the decrease is not as large. We also find that the O^+ percentage at high altitudes under sunlit conditions is lowest when the photoelectrons are switched off, and highest when the both photoelectrons and the enhanced O^+ production rate are included. The agreement with the empirical model of *Kitamura et al.* [2011] is best when both mechanisms are included and worst when the photoelectrons are neglected. From this analysis we conclude that the photoelectrons play somewhat a larger role than the enhanced O^+ production rate in describing the differences between sunlit and dark conditions, however both are needed to adequately reproduce the data.

[34] It is also instructive to qualitatively compare our results with those of *Demars and Schunk* [2001]. They use a model similar to the full-size PWOM that follows over 1000 convecting flux tubes for a variety of seasonal, solar cycle, and geomagnetic conditions. As they do not include the direct effects of photoelectrons, the comparison helps to further isolate the contribution of the photoelectrons. Examination of the result presented by *Demars and Schunk* [2001] indicate some increase in O^+ density for low SZA that is not related to the aurora. That effect is still visible but less pronounced at 8,000 km. Overall, the increase in O^+ under sunlit conditions at 2,000 and 8,000 km is less clear than in our study that includes photoelectrons. This is consistent with our results in Figure 9 which demonstrates that increased O^+ production rate under sunlit conditions accounts for some of the sunlit-dark asymmetry, but including photoelectrons helps O^+ reach higher altitudes. An interesting point raised by *Demars and Schunk* [2001] is that during a geomagnetic storm, the O^+ density can become

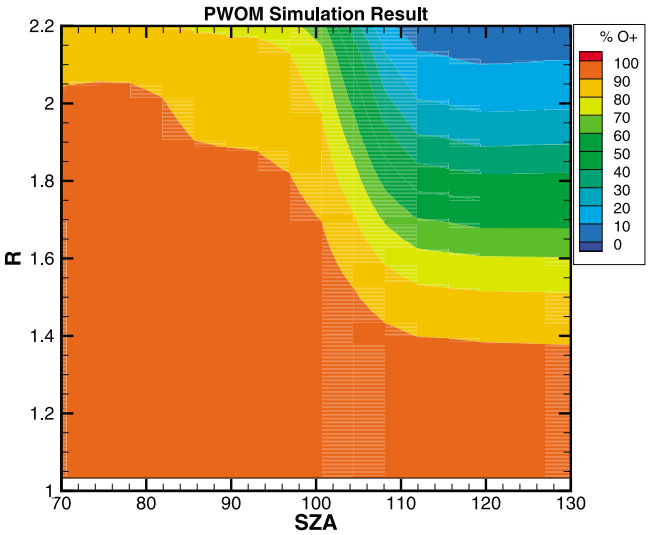

Figure 7. A color contour of the percent of O^+ as a function of SZA and radial distance. O^+ is the dominant ion at all altitudes under sunlit conditions, while H^+ becomes the dominant ion under dark conditions. A sharp transition is seen across the terminator.

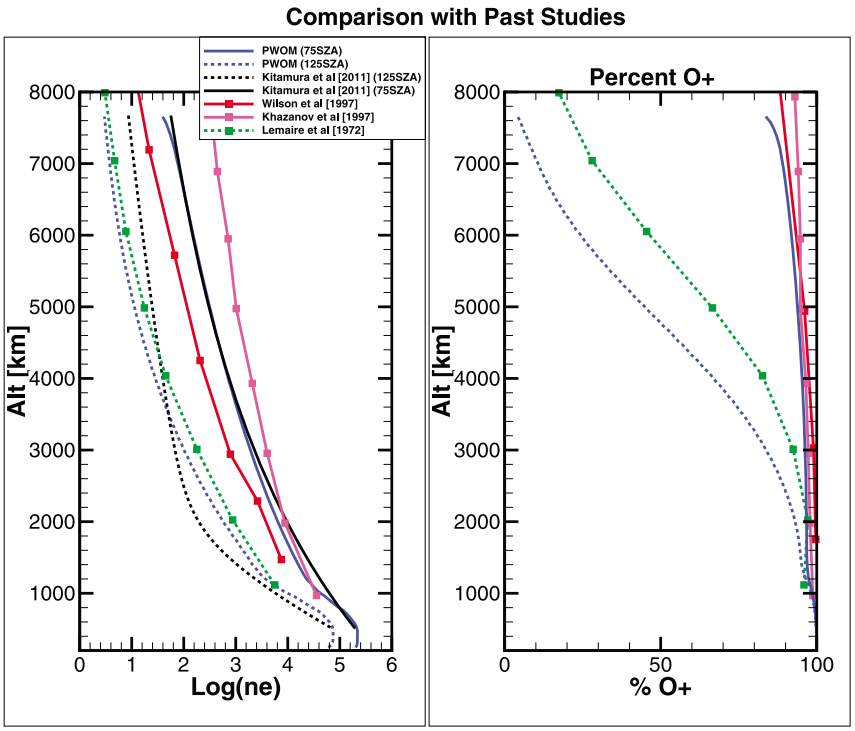

Figure 8. A direct comparison as a function of SZA at fixed altitude between the PWOM calculation (blue) and past studies by *Lemaire* [1972] (green), *Khazanov et al.* [1997] (pink), and *Wilson et al.* [1997] (red). The empirical result from *Kitamura et al.* [2011] is included as a reference. Results for sunlit conditions are solid lines and results for dark conditions are dashed lines.

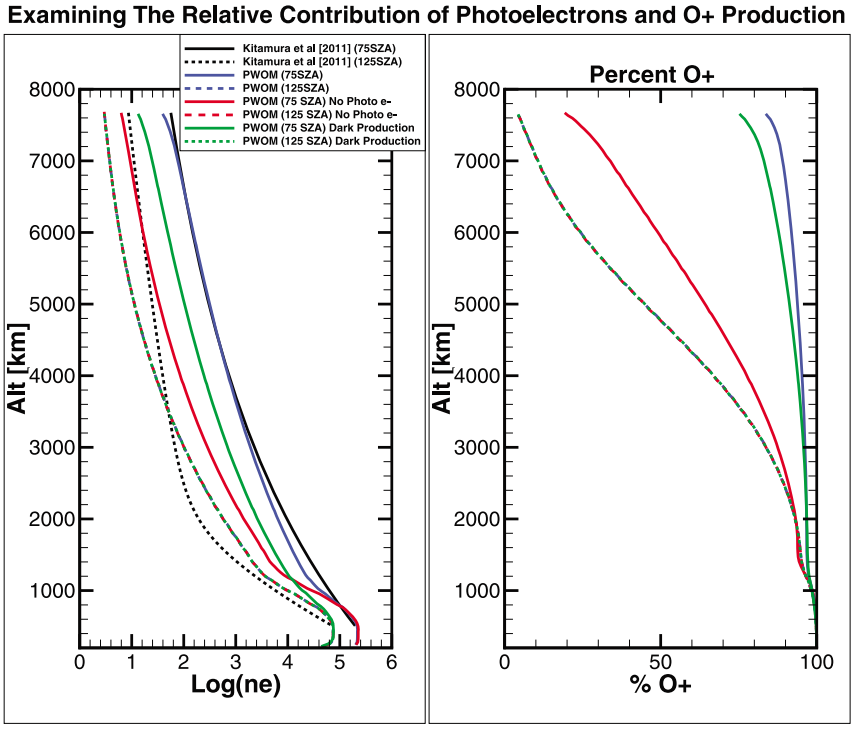

Figure 9. Altitude profiles of (left) the log of electron number density and (right) O^+%. The lines represent the empirical model of *Kitamura et al.* [2011] (black), our PWOM simulation (blue), PWOM simulation with no photoelectrons (red), and PWOM with photoelectron but with the O^+ production rate set to dark values. Sunlit solutions are shown with solid lines and dark solutions are shown with dashed lines.

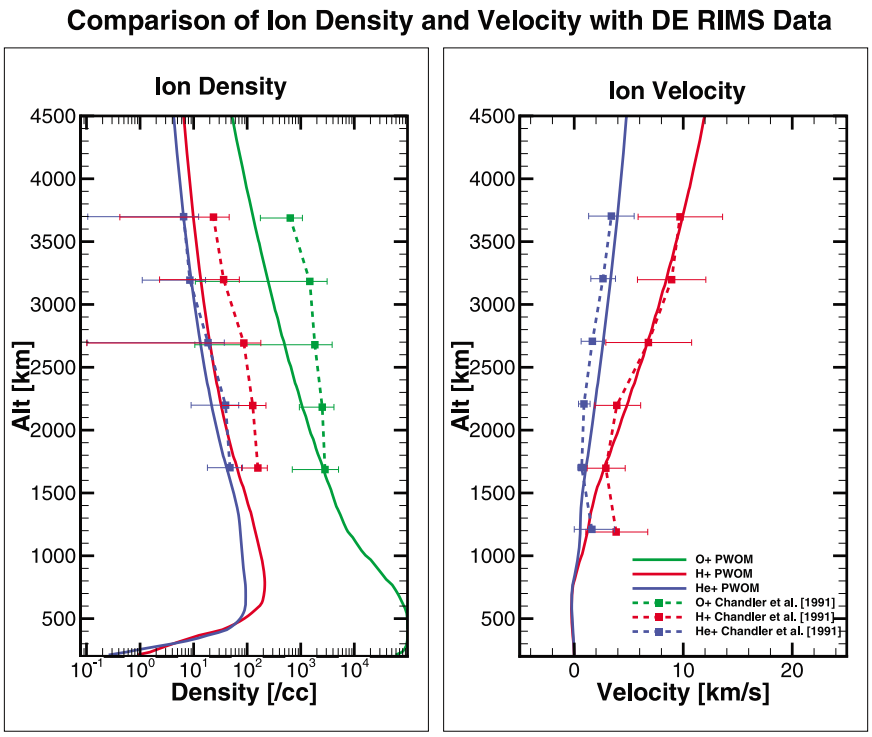

Figure 10. A comparison of our PWOM simulation (solid lines) with DE-RIMS from *Chandler et al.* [1991] (squares connected by dashed lines). (left) The altitude profiles of the ion densities and (right) the altitude profiles of the ion velocities. O^+ is shown in green, H^+ is shown in red, and He^+ is shown in blue.

large throughout the entire polar cap. This results appears to be irrespective of SZA. As a consequence, we recognize that photoelectrons have to compete with other effects during active times. Although active times are beyond the scope of the present study, we note that photoelectrons at a minimum influence the quiet time initial state of the polar wind, and increases the available O^+ density at high altitude to be further energized by other mechanisms.

[35] We further compare our results to studies of ion density and velocity in the polar wind using DE and Akebono data. Figure 10 presents a direct comparison between our PWOM simulation and average DE-RIMS data presented by *Chandler et al.* [1991]. Altitude profiles of ion density are shown in Figure 10 (left), and profiles of ion velocity are shown in Figure 10 (right). O^+ is shown in green, H^+ is shown in red, and He^+ is shown in blue. The PWOM simulation (averaged over the entire domain for each altitude) is shown in solid lines, the DE data from *Chandler et al.* [1991] is shown in the square symbols with error bars connected with dashed lines. The ion velocities seem to agree well at all altitudes, although some small difference is seen at the lowest altitude. The ion densities are consistently lower than the data, but are generally within the (rather large) error bars. Some caution is required when comparing our simulation with the data presented by *Chandler et al.* [1991] since their study does not consider the effect of geomagnetic activity. They do note that flux shows a variation of about a factor of 3 over the range of Kp (from 0 to −7). Additionally, our simulation is for F10.7 set to 200, while the study of *Chandler et al.* [1991] has F10.7 > 190. Despite the caveats and the noted differences in the densities, our results are consistent with those of *Chandler et al.* [1991].

[36] Figure 11 presents a direct comparison of altitude profiles of velocity between our PWOM simulation and the study of *Abe et al.* [2004] based on Akebono data. Figure 11 (left) shows results for sunlit conditions (SZA < 90°), and Figure 11 (right) shows results for dark conditions (SZA > 90). The PWOM simulation is averaged for SZA < 90° and SZA > 90° to get the sunlit and dark conditions most appropriate for comparison to the study of *Abe et al.* [2004]. The simulated H^+ velocity is shown in red, and the simulated O^+ is shown in green. The O^+ velocity from *Abe et al.* [2004] is shown in cyan and the H^+ velocity is shown in blue. We choose the results for F10.7 = 180–300 from *Abe et al.* [2004] as being the most appropriate to our study. The O^+ velocity in the simulation is largely consistent with the Akebono data presented by *Abe et al.* [2004]. However, the H^+ velocity begins to differ significantly above 3,000 km under sunlit conditions and above 2,000 km under dark conditions. We note that reducing the topside electron heat flux does reduce the H^+ velocity somewhat under dark conditions, but not enough to constitute a good agreement with the data (see dashed red line). A further reduction of the topside heat flux may improve this comparison, but it is unlikely to eliminate the error, particularly under sunlit conditions which are less sensitive to this parameter. It is likely that kinetic processes, known to be important at high altitudes, may play a role. Testing this theory requires a model that includes kinetic effects (such as the macroscopic particle-in-cell code of *Barakat and Schunk*

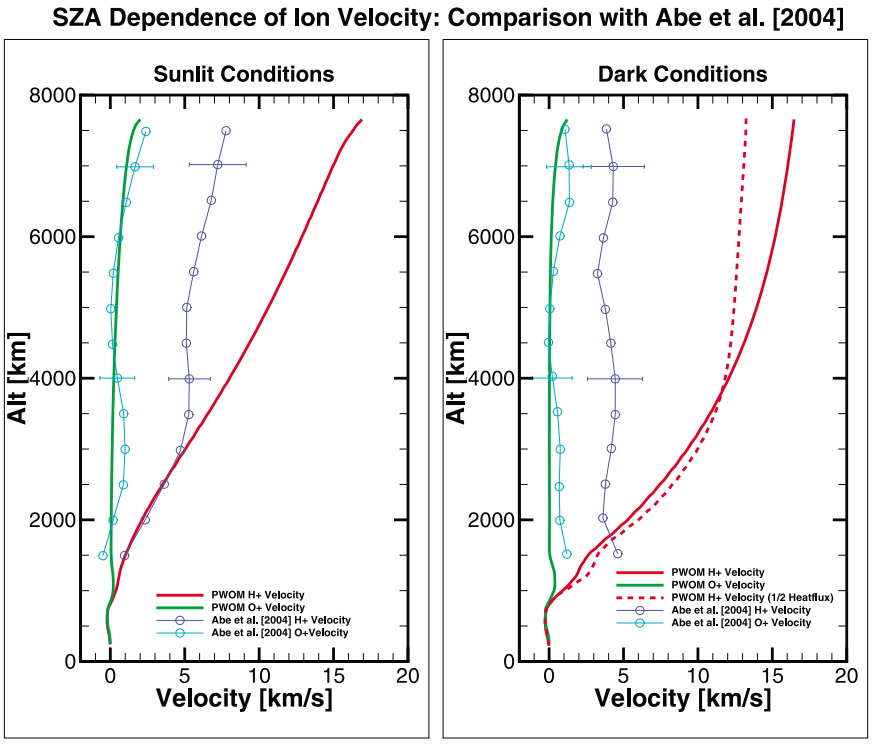

Figure 11. A comparison between our PWOM simulation and the study of *Abe et al.* [2004] based on Akebono data. The simulated H^+ velocity is shown in red, and the simulated O^+ is shown in green. The O^+ velocity from *Abe et al.* [2004] is shown in cyan, and the H^+ velocity is shown in blue.

[2006]), but is beyond the current capabilities of our model. Further investigation of the discrepancy between the modeled and observed H^+ velocity will clearly require additional study.

4. Discussion and Conclusion

[37] We have expanded the PWOM to include the effects of photoelectrons. Our newly improved model was then used to study SZA effects on the polar wind during geomagnetically quiet times at solar maximum. The model's results were compared with an empirical model of the electron density and ion and electron temperature measurements from ESR and IK satellites [*Kitamura et al.*, 2011]. We draw several conclusions from these data model comparisons.

[38] First, the change in the vertical profile of the electron density between sunlit and dark conditions is largely driven by two different but closely tied mechanisms, namely, photoelectrons and the enhancement of the O^+ production rate with photoelectrons playing a somewhat larger role. The photoelectron inputs to the model (see Figure 2) show a clear drop in the photoelectron flux and energy around 100° SZA. That drop corresponds to a marked transition in the electron density across the terminator. This change is seen in both the data based empirical model and the PWOM result. While a change across the terminator is also seen in the model when the photoelectrons are not included, it is not as strong.

[39] The electron temperatures, and, to a lesser degree, the ion temperatures in ESR and IK data as well as the PWOM simulation are found to drop significantly in the transition from sunlit to dark conditions. This result is consistent with that of *Khazanov et al.* [1997] who demonstrated that increased photoelectron concentrations can result in larger electron temperatures.

[40] We further find that photoelectrons play a large role in defining the ion composition at high altitudes. Under sunlit conditions, where there are significant photoelectron fluxes, we demonstrate that O^+ is the dominant ion to at least 8,000 km. In contrast, under dark conditions H^+ is dominant at high altitudes. These results are shown to be in good agreement with past models of *Khazanov et al.* [1997], *Wilson et al.* [1997], and *Lemaire* [1972].

[41] This point is extremely interesting as it is often asserted that O^+ is required to reach about 11.2 km/s in order to escape Earth's gravitation. Therefore we should not expect much O^+ at high altitudes without an energization mechanism. However, *Moore and Khazanov* [2010] pointed out that this idea ignores the ambipolar potential that can arise from a superthermal electron population. Including such a population reduces the potential barrier faced by O^+. While this may not result in large fluxes, it can enable significant quantities of O^+ to reach high altitudes.

[42] Other explanations for the change in vertical profile of the electron density across the terminator are found to be implausible. These are geomagnetically quiet times, and the empirical model of *Kitamura et al.* [2011] excludes the cusp and auroral regions; wave-particle interactions are most intense during active times and in the cusp and auroral regions. Therefore the effect of wave-particle interactions should be reduced in these results. However, as noted by *Barghouthi* [1997], wave-particle interactions may still reach significant levels in the polar cap, particularly at high altitudes. Additionally these are times of slow convection so

Joule heating is low; we actually turned this term off in the simulation and saw little effect. Finally, in these simulations we used a value of the topside electron heat flux that is constant everywhere in the modeled domain (no change across the terminator). Since this quantity is ill-constrained do to lack of measurements, we chose a value (3.75×10^{-4} ergs cm^{-2} s^{-1} at 8000 km altitude) that results in electron temperatures consistent with observations on the nightside. We also tried a case with half the amount of topside electron heat flux. These results are shown in Figure 3c and the dashed lines in Figures 4, 5, and 6. The sunlit solution was only very slightly affected, demonstrating that topside electron heat flux had very little impact in this region. The solution under dark conditions was altered; the electron temperature dropped significantly as did the scale height of the electrons and ions. We therefore conclude that under sunlit conditions the photoelectrons have a controlling effect, while under dark conditions the value of the topside electron heat flux is more important.

[43] Finally, this study has served as an initial validation of the PWOM's ability to simulate the geomagnetically quiet polar wind solution. A more complete (and difficult) validation involving data model comparisons during actual events with the full model capabilities is still needed, but is deferred to future studies. We have directly compared our model's results to an empirical model of electron density derived from Akebono measurements and to a statistical compilation of ion and electron temperature from ESR and IK satellites presented by *Kitamura et al.* [2011]. Additionally, we compared our results with ion densities and velocities from DE-RIMS presented by *Chandler et al.* [1991] and Akebono presented by *Abe et al.* [2004]. Overall, the data model comparison was found to be reasonable although some notable discrepancies exist. For example:

[44] 1. The observed electron temperature stays almost constant above 500 km, while the computed temperature profile continues to rise with altitude.

[45] 2. At 8,000 km, the difference between the empirical and the computational models is relatively large.

[46] 3. The H^+ velocity above 3,000 km under sunlit conditions and 2,000 km under dark conditions exceeds those reported by *Abe et al.* [2004] by a factor of 2–3.

[47] These discrepancies maybe due to the limitations inherent to the fluid-like approach used in our model, and the high-altitude processes that are missing from it. They may also be connected to the simplification of holding the field lines stationary. As we continue to improve the model in our future development we hope these discrepancies will diminish.

[48] **Acknowledgments.** Resources supporting this work were provided by the NASA High-End Computing (HEC) Program through the NASA Advanced Supercomputing (NAS) Division at Ames Research Center and the NASA Center for Climate Simulation (NCCS) at Goddard Space Flight Center.

[49] Robert Lysak thanks the reviewers for their assistance in evaluating this paper.

References

Abe, T., B. A. Whalen, A. W. Yau, R. E. Horita, S. Watanabe, and E. Sagawa (1993), EXOS D (Akebono) suprathermal mass spectrometer observations of the polar wind, *J. Geophys. Res.*, *98*(A7), 11,191–11,203, doi:10.1029/92JA01971.

Abe, T., A. W. Yau, S. Watanabe, M. Yamada, and E. Sagawa (2004), Long-term variation of the polar wind velocity and its implication for the ion acceleration process: Akebono/suprathermal ion mass spectrometer observations, *J. Geophys. Res.*, *109*, A09305, doi:10.1029/2003JA010223.

Axford, W. I. (1968), The polar wind and the terrestrial helium budget, *J. Geophys. Res.*, *73*, 6855–6859, doi:10.1029/JA073i021p06855.

Banks, P. M., and T. E. Holzer (1968), The polar wind, *J. Geophys. Res.*, *73*, 6846–6854, doi:10.1029/JA073i021p06846.

Banks, P. M., and A. F. Nagy (1970), Concerning the influence of elastic scattering upon photoelectron transport and escape, *J. Geophys. Res.*, *75*, 1902–1910, doi:10.1029/JA075i010p01902.

Barakat, A. R., and R. W. Schunk (1983), O^+ ions in the polar wind, *J. Geophys. Res.*, *88*, 7887–7894, doi:10.1029/JA088iA10p07887.

Barakat, A. R., and R. W. Schunk (2006), A three-dimensional model of the generalized polar wind, *J. Geophys. Res.*, *111*, A12314, doi:10.1029/2006JA011662.

Barghouthi, I. A. (1997), Effects of wave-particle interactions on H^+ and O^+ outflow at high latitude: A comparative study, *J. Geophys. Res.*, *102*, 22,065–22,076, doi:10.1029/96JA03293.

Brinton, H. C., J. M. Grebowsky, and H. G. Mayr (1971), Altitude variation of ion composition in the midlatitude trough region: Evidence for upward plasma flow, *J. Geophys. Res.*, *76*, 3738–3745, doi:10.1029/JA076i016p03738.

Burgers, J. M. (1969), *Flow Equations for Composite Gases*, Academic, New York.

Chandler, M. O., T. E. Moore, and J. H. Waite Jr. (1991), Observations of polar ion outflows, *J. Geophys. Res.*, *96*, 1421–1428, doi:10.1029/90JA02180.

Demars, H. G., and R. W. Schunk (2001), Seasonal and solar cycle variations of the polar wind, *J. Geophys. Res.*, *106*, 8157–8168, doi:10.1029/2000JA000386.

Ganguli, S. B., H. G. Mitchell, and P. J. Palmadesso (1987), Behavior of ionized plasma in the high latitude topside ionosphere: The polar wind, *Planet. Space Sci.*, *35*, 703–714, doi:10.1016/0032-0633(87)90030-4.

Glocer, A., T. I. Gombosi, G. Toth, K. C. Hansen, A. J. Ridley, and A. Nagy (2007), Polar wind outflow model: Saturn results, *J. Geophys. Res.*, *112*, A01304, doi:10.1029/2006JA011755.

Glocer, A., G. Toth, T. Gombosi, and D. Welling (2009a), Modeling ionospheric outflows and their impact on the magnetosphere, initial results, *J. Geophys. Res.*, *114*, A05216, doi:10.1029/2009JA014053.

Glocer, A., G. Tóth, Y. Ma, T. Gombosi, J. Zhang, and L. M. Kistler (2009b), Multifluid Block-Adaptive-Tree Solar wind Roe-type Upwind Scheme: Magnetospheric composition and dynamics during geomagnetic storms—Initial results, *J. Geophys. Res.*, *114*, A12203, doi:10.1029/2009JA014418.

Gombosi, T. I., and A. Nagy (1989), Time-dependent modeling of field-aligned current-generated ion transients in the polar wind, *J. Geophys. Res.*, *94*, 359–369, doi:1031029/JA094iA01p00359.

Hedin, A. (1983), A revised thermospheric model based on mass spectometer and incoherent scatter data: MSIS-83, *J. Geophys. Res.*, *88*, 10,170–10,188, doi:10.1029/JA088iA12p10170.

Hedin, A. (1987), MSIS-86 thermospheric model, *J. Geophys. Res.*, *92*, 4649–4662, doi:1031029/JA092iA05p04649.

Hedin, A. (1991), Extension of the MSIS thermosphere model into the middle and lower atmosphere, *J. Geophys. Res.*, *96*, 1159–1172, doi:10.1029/90JA02125.

Hoffman, J. H. (1970), Studies of the composition of the ionosphere with a magnetic deflection mass spectrometer, *Int. J. Mass Spectrom. Ion Phys.*, *4*, 315–322.

Hoffman, J. H., W. H. Dodson, C. R. Lippincott, and H. D. Hammack (1974), Initial ion composition results from the Isis 2 satellite, *J. Geophys. Res.*, *79*, 4246–4251, doi:10.1029/JA079i028p04246.

Khazanov, G. V., M. W. Liemohn, and T. E. Moore (1997), Photoelectron effects on the self-consistent potential in the collisionless polar wind, *J. Geophys. Res.*, *102*, 7509–7522, doi:10.1029/96JA03343.

Kitamura, N., Y. Ogawa, Y. Nishimura, N. Terada, T. Ono, A. Shinbori, A. Kumamoto, V. Truhlik, and J. Smilauer (2011), Solar zenith angle dependence of plasma density and temperature in the polar cap ionosphere and low-altitude magnetosphere during geomagnetically quiet periods at solar maximum, *J. Geophys. Res.*, *116*, A08227, doi:10.1029/2011JA016631.

Lee, J. S., J. P. Doering, T. A. Potemra, and L. H. Brace (1980), Measurements of the ambient photoelectron spectrum from atmosphere explorer: II. AE-E measurements from 300 to 1000 km during solar minimum conditions, *Planet. Space Sci.*, *28*, 973–996, doi:10.1016/0032-0633(80)90059-8.

Lemaire, J. (1972), Effect of escaping photoelectrons in a polar exospheric model, *Space Res.*, *12*, 1413–1416.

Mitchell, H. G., and P. J. Palmadesso (1983), A dynamic model for the auroral field line plasma in the presence of field-aligned current, *J. Geophys. Res.*, *88*, 2131–2139, doi:10.1029/JA088iA03p02131.

Moore, T. E., and G. V. Khazanov (2010), Mechanisms of ionospheric mass escape, *J. Geophys. Res.*, *115*, A00J13, doi:10.1029/2009JA014905.

Nagai, T., J. H. Waite Jr., J. L. Green, C. R. Chappell, R. C. Olsen, and R. H. Comfort (1984), First measurements of supersonic polar wind in the polar magnetosphere, *Geophys. Res. Lett.*, *11*, 669–672, doi:10.1029/GL011i007p00669.

Peterson, W. K., T. N. Woods, P. C. Chamberlin, and P. G. Richards (2008), Photoelectron flux variations observed from the FAST satellite, *Adv. Space Res.*, *42*, 947–956, doi:10.1016/j.asr.2007.08.038.

Schunk, R. W. (1981), Electron temperature anisotropy in the polar wind, *J. Geophys. Res.*, *86*, 91–102, doi:10.1029/JA086iA01p00091.

Schunk, R. W., and A. F. Nagy (2000), *Ionospheres: Physics, Plasma Physics, and Chemistry*, Cambridge Univ. Press, Cambridge, U. K.

Schunk, R. W., and D. S. Watkins (1982), Proton temperature anisotropy in the polar wind, *J. Geophys. Res.*, *87*, 171–180, doi:10.1029/JA087iA01p00171.

Su, Y.-J., J. L. Horwitz, G. R. Wilson, P. G. Richards, D. G. Brown, and C. W. Ho (1998), Self-consistent simulation of the photoelectron-driven polar wind from 120 km to 9 Re altitude, *J. Geophys. Res.*, *103*, 2279–2296, doi:10.1029/97JA03085.

Tam, S. W. Y., F. Yasseen, T. Chang, and S. B. Ganguli (1995), Self-consistent kinetic photoelectron effects on the polar wind, *Geophys. Res. Lett.*, *22*, 2107–2110, doi:10.1029/95GL01846.

Tam, S. W. Y., F. Yasseen, and T. Chang (1998), Further development in theory/data closure of the photoelectron-driven polar wind and day-night transition of the outflow, *Ann. Geophys.*, *16*, 948–968, doi:10.1007/s00585-998-0948-2.

Waite, J. H., Jr., et al. (1985), Escape of suprathermal O^+ ions in the polar cap, *J. Geophys. Res.*, *90*, 1619–1630, doi:10.1029/JA090iA02p01619.

Wilson, G. R., G. Khazanov, and J. L. Horwitz (1997), Achieving zero current for polar wind outflow on open flux tubes subjected to large photoelectron fluxes, *Geophys. Res. Lett.*, *24*, 1183–1186, doi:10.1029/97GL00923.

A. Glocer, NASA GSFC, Code 673, Greenbelt, MD 20771, USA. (alex.glocer-1@nasa.gov)

T. Gombosi and G. Toth, Department of Atmospheric Oceanic and Space Science, University of Michigan, Ann Arbor, Michigan, USA.

N. Kitamura, Department of Geophysics, Tohoku University, 6-3 Aramaki-aza-Aoba, Sendai, 980-8578 Japan.